ACS OMEGA

Open Access

http://pubs.acs.org/journal/acsodf

Article

Adjoint-Optimized Large Dielectric Metasurface for Enhanced Purcell Factor and Directional Photon Emission

Erfan Khoram,* Zongfu Yu, and S. Ali Hassani Gangaraj

Cite This: *ACS Omega* 2024, 9, 24356−24361

Read Online

ACCESS | Metrics & More | Article Recommendations | Supporting Information

ABSTRACT: Extracting photons efficiently from quantum sources, such as atoms, molecules, and quantum dots, is crucial for various nanophotonic systems used in quantum communication, sensing, and computation. To improve the performance of these systems, it is not only necessary to provide an environment that maximizes the number of optical modes, but it is also desirable to guide the extracted light toward specific directions. One way to achieve this goal is to use a large area metasurface that can steer the beam. Previous work has used small aperture devices that are fundamentally limited in their ability to achieve high directivity. This work proposes an adjoint-based topology optimization approach to design a large light extractor that can enhance the spontaneous decay rate of the embedded quantum transition and collimate the extracted photons. With the help of this approach, we present all-dielectric metasurfaces for a quantum transition emitting at λ = 600 nm. These metasurfaces achieve a broadband improvement of spontaneous emission compared to that in the vacuum, reaching a 10× enhancement at the design frequency. Furthermore, they can beam the extracted light into a narrow cone (±10°) along a desired direction that is predefined through their respective design process.

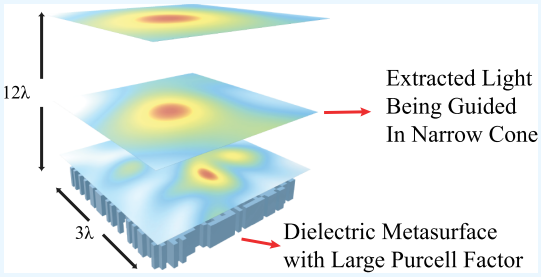

INTRODUCTION

When employing quantum emitters (atoms, molecules, quantum dots, etc.), it is essential that photon extraction efficiency from them is maximized and the extracted photons are properly guided. This requisite is made evident in many applications. For instance, in quantum sensing, it is paramount that photons emitted from a source are guided outside the solid-state structure and into narrow cones, as measurement sensitivity and the resolution of such systems are limited by the number of collected photons; moreover, improved photon extraction can lead to increased signal-to-noise ratio and detection efficiency for such sensors. In quantum transport problems, the same requirements present themselves when two quantum transitions need to have strong dipole−dipole coupling.[1,2] Maximizing the efficiency of light extraction is directly linked to enhancing spontaneous emission, which is a measure of available optical modes for emitted photons. Fortunately, we have come to understand that the spontaneous emission of a quantum emitter can be modified by engineering its photonic reservoir.[3] Therefore, to enhance the extraction of photons from an emitter (Figure 1a), the medium around it must provide an ample number of optical modes for the photons to occupy. This can be done by simply placing the emitter inside a dielectric (Figure 1b); however, doing so puts a fundamental upper limit on the enhancement ratio equal to the refractive index of the host material. An intelligent design of the mechanisms constituting the environment around the emitter can surpass such a limit. Among other methods, this has been achieved by utilizing micro/nanocavities that the emitter would be in resonance with,[4−6] or metallic nanostructures that amplify the spontaneous emission.[7,8] Effective as these methods are, introducing resonance-based phenomena limits the bandwidth of the embedded quantum

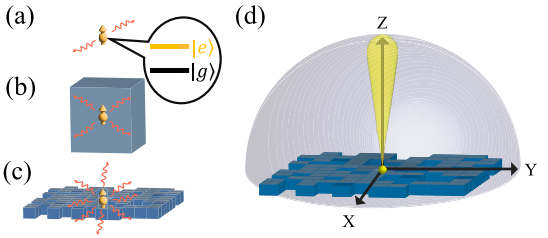

Figure 1. (a) A quantum transition at vacuum, emitting photons. (b) Enhanced decay rate achieved by placing the two level system inside an infinite environment filled with a dielectric is limited by the refractive index of that dielectric. (c) Better enhancement can be achieved by placing the quantum transition inside a deliberately engineered metasurface. (d) The metasurface can simultaneously guide the extracted photons inside narrow beams toward specific directions.

Received: December 25, 2023
Revised: April 27, 2024
Accepted: May 8, 2024
Published: May 28, 2024

sources, which nulls the broadband advantages of solid-state emitters; while using metal-based elements in the design instigates undesirable loss to the system. An alternative avenue toward the same goal is to employ dielectric metasurfaces, which can overcome the emitter's bandwidth issue, and the system's energy loss while providing the same degrees of control as their metallic counterparts.[9] An approach that has proven itself to be extremely effective in designing complex analog systems (e.g., systems capable of solving differential equations[10] or running neural inference on time-domain data[11]) and photonic quantum systems[12−15] is topology optimization through the adjoint method. Such a target-oriented design perspective not only helps us to enhance the decay rate of emission but also allows us to precisely define the direction of the extracted photons, which also has a variety of applications. For instance, in quantum communication, controlling the emission direction of photons is critical for ensuring reliable transmission over long distances. This is similarly done by engineering the host medium in such a way that the electromagnetic interaction of the outgoing light with it morphs the light into a desired beam. Addressing these two differing goals requires us to take a multiobjective optimization approach as taken by many inverse design works aiming to address multiple challenges at once.[13,16,17] Consequently, we, too, present a multiobjective optimization scheme based on the adjoint method to design a large all-dielectric metasurface that simultaneously increases the Purcell factor (an indicator of the number of optical modes available to the emitted photon) and precisely guides the extracted light into narrow cones along specific directions. As described above, such a combination of enhanced spontaneous emission and directional photon emission opens opportunities for advancing various optical and quantum technologies.

Furthermore, we use our proposed process to inversely design two Si-based structures, with a quantum transition placed in the center as the source. While both of these designs provide a 10× enhancement of the spontaneous emission at the wavelength of interest (λ = 600 nm) and guide the extracted light inside a narrow cone 10° wide, each of their corresponding cones points to different directions (one guides the light along the z-axis and the other along a direction 40° off that axis).

METHODS

In this work, we designed silicon-based large metasurfaces that can act as light extractors. The objectives these designs have to clear are achieving large Purcell factor enhancement for the embedded quantum transition and beaming the extracted light into narrow cones in the far-field. Through the lens of topology optimization, these objectives are mapped to target behaviors, characterized by numerical values, inside a cost function that contrasts the performance of a given design to it. Although there are packages such as Meep that implement topology optimization in near- and far-field domains,[18] here we use Tidy3D, a hardware-accelerated FDTD solver designed to handle large electromagnetic simulations considerably faster than other solvers.[19] While this allows us to potentially design very large photonic media in a fast and efficient manner, it also means we have to derive and implement the back-propagation step of the optimization process (see Supporting Information). The first stated goal can be rephrased as the enhancement of spontaneous emission of the emitter in the metasurface compared with the vacuum. The spontaneous decay rate of a single emitter is linked to the local density of states of its environment, representing the number of available electromagnetic modes for photon emission.[20,21] At the location of the emitter, the spontaneous emission is directly proportional to the imaginary part of the system's Green function ($I(G)$) of the wave equation evaluated at the emitter's location.[1,22] As a result, the enhancement ratio of the decay rate, i.e. Purcell factor (PF) becomes the ratio of the imaginary part of the Green function of the emitter inside the designable structure ($I(G_s)$) over that of the vacuum ($I(G_0)$), both evaluated at the quantum transition's position (since this work takes on an electromagnetics-based model for light propagation, we also use a classic description for defining the Purcell factor; therefore we have implemented PF as the ratio of the real part of the electric field at the location of the emitter between the two environments). In order to increase PF during the optimization process, we try to minimize its difference with a large target value $\mathrm{PF_t}$. As a result, the cost function representing this aspect of the target behavior becomes

$$C_{\mathrm{pf}} = \left(\frac{I(G_s)}{I(G_0)} - \mathrm{PF_t}\right)^2 \tag{1}$$

The second goal for the presented task is to guide the extracted light through narrow beams along specific directions. This goal is defined in terms of the far-field radar pattern of our designable metasurface ($y_{(\theta,\phi)}$): we equate the precise directing of the extracted photons to the formation of narrow beams in the far-field pattern. For such a narrow beam, the ideal distribution of $\tilde{y}$ ($y_{(\theta,\phi)}$ normalized by its maximum value $\|y\|_\infty$ over all angles θ and ϕ) would be near-one values for angles close to the peak of the beam followed by a sudden drop to near-zero values further from the beam center. This can be encouraged in the inverse-design process by introducing the target behavior $\tilde{y}_{\mathrm{t}(\theta,\phi)}$ that takes values equal to 1 for the specific angles where the beam is aiming toward, and zero elsewhere. Consequently, the design can be optimized for this desired behavior by minimizing the following cost function.

$$C_{\mathrm{ff}} = \int_0^{2\pi}\int_0^{\pi/2}\left(\frac{y_{(\theta,\phi)}}{\|y\|_\infty} - \tilde{y}_{\mathrm{t}(\theta,\phi)}\right)^2 \mathrm{d}\theta\mathrm{d}\phi \tag{2}$$

The full cost function C for our desired metasurfaces is a linear combination of the terms presented in eqs 1 and 2. This cost function then has to be minimized with the electromagnetic wave equation (for near- and far-field) as a constraint. This optimization problem can be formulated in the following format, where $Ae = b$ represents the frequency domain wave equation (with A, e, and b being the electromagnetic wave operator, the electric-field vector, and the source vector, respectively).

$$\begin{aligned} &\text{minimize } C = vC_{\mathrm{pf}} + wC_{\mathrm{ff}} \\ &\text{subject to } Ae = b \end{aligned} \tag{3}$$

where the weights v and w are meant to keep both terms in the cost function on the same order of magnitude. As hinted at in Figure 1, the photonic media designed in this work are pixelated binary metasurfaces. To design for such metasurfaces, we employ a density-based topology optimization approach where the density function is defined in terms of a linear combination of b-spline functions, and the adjoint method computes the gradient of that cost function with respect to the

https://doi.org/10.1021/acsomega.3c10362
ACS Omega 2024, 9, 24356−24361

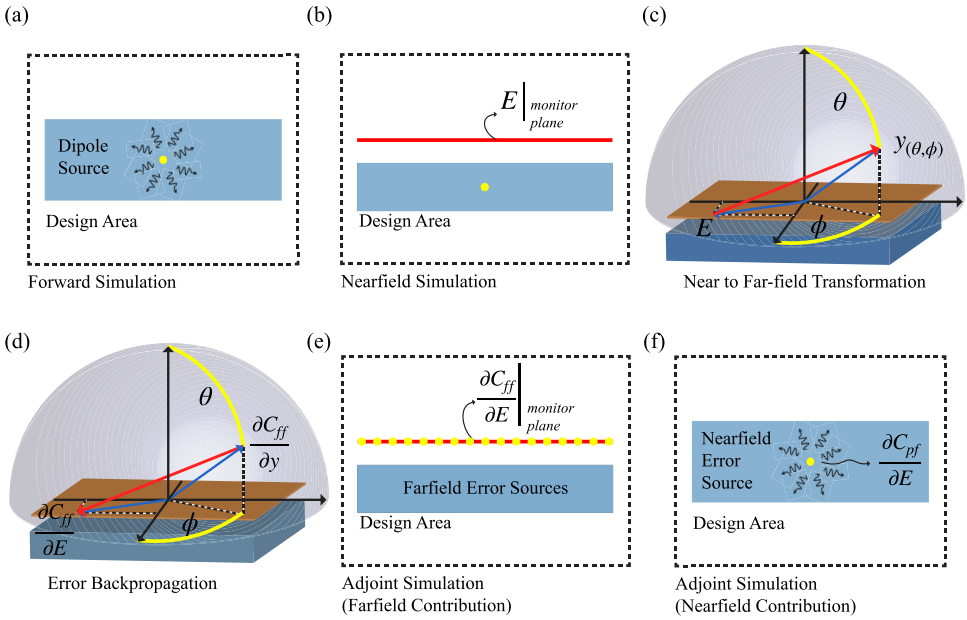

Figure 2. (a) In the setup for modeling the near-field regime of the forward problem, the dipole representing the quantum transition is placed in the center of the designable metasurface. The electric field is then measured (b) at the location of the source to compute the enhancement ratio of the decay rate, and on a monitor plane above the metasurface, which is then used for (c) the near-to-far-field transformation. (d) For modeling the backward problem, the gradient of the cost function w.r.t the far-field has to be first transformed to the gradient of the cost function to the near-field. Then, the corresponding near-field error sources for (e) far-field and (f) the near-field can be placed.

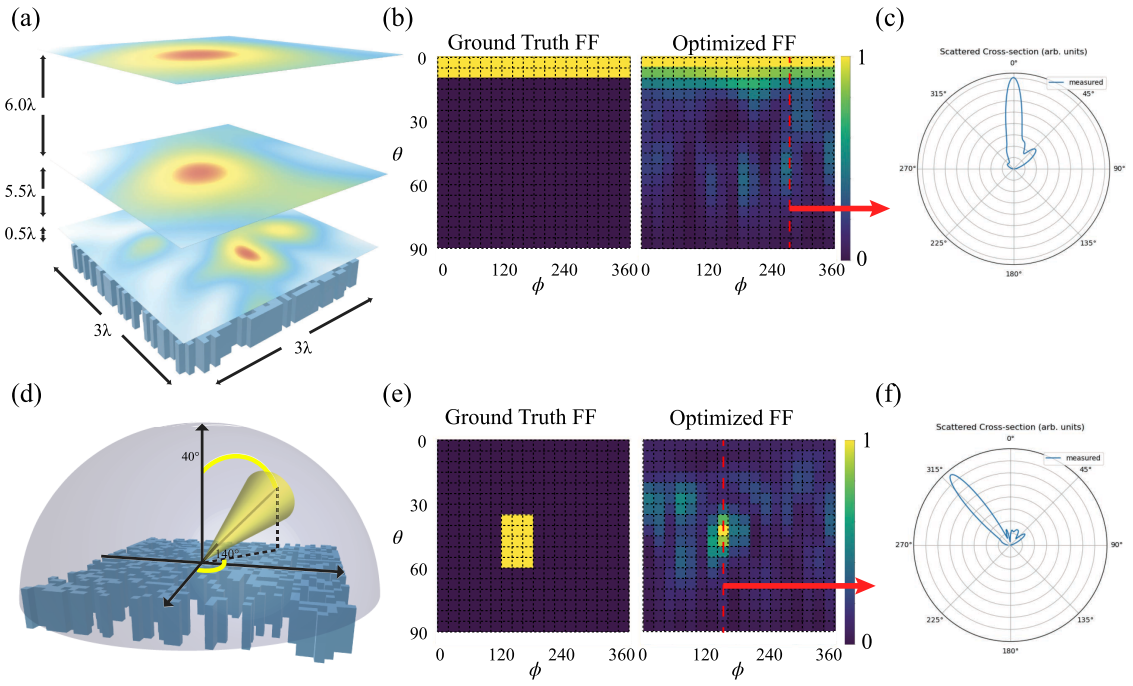

Figure 3. Two structures with a 10× enhancement of spontaneous emission at $\lambda = 600$ nm. (a) The first structure guides light perpendicular to its surface in a narrow cone, while (b) the second structure directs light to a cone 40° off this axis. (c, d) The comparison between the far-field performance and the target response for each of the two designs. (e, f) The radar pattern for the two designs at $\phi = 45°$ and $\phi = 140°$, respectively.

coefficients of that linear combination.[23,24] In general, b-splines enable the generation of complex binary media with smooth curved boundaries between the two materials, with controllable feature sizes.[23] In the case of pixelated media, as is the case here, this translates to modifying the pixel sizes in the design. This allows us to change the dimensions of our building blocks to suit the target performance (see Supporting Information).

In a design with many tunable parameters (p), the adjoint method allows us to compute the contribution of all of them by solving one extra equation (eq 4) called the adjoint equation. Here, A^T is the transpose of the electromagnetic wave operator matrix, e^{adj} is the adjoint field, and $\nabla_e C$ is the gradient of the cost function with respect to the electric field, and it is nonzero only where the field is measured for each term in the cost function.

https://doi.org/10.1021/acsomega.3c10362
ACS Omega 2024, 9, 24356−24361

$$A^{T}e^{adj} = \nabla_{e}C \tag{4}$$

The necessary gradients for the optimization are the real part of the Hadamard product between the electric field and its corresponding adjoint field (see[24,25] for detailed derivation).

$$\nabla_{p}C = R(e \odot e^{adj}) \tag{5}$$

While previous works have shown that spontaneous emission can be enhanced using intricately designed small-scale metasurfaces,[14] we intuit that a larger design allows for more precisely guiding the extracted photons. However, accurate modeling of large photonic media can be very computationally expensive. In order to address this issue, as mentioned earlier, we use Tidy3D. Using this solver, we model the forward problem (solving for the electric field) in the near-field regime (Figure 2a). This allows us to compute the enhancement ratio of the decay rate by measuring the field at the location of the source (Figure 2b) and to compute the far-field by measuring the field on a plane above the metasurface, and then applying a near-to-far-field transformation[26] to it (Figure 2c). Modeling the forward problem will be complete once we compute the value of the full cost function C corresponding to a given design.

The next stage is modeling the adjoining problem (solving for the adjoint field). For this stage, Tidy3D proves useful. This is possible because the wave operator A is symmetric for the most part. As a result, the adjoint eq (eq 4) can also be posed as an electromagnetic simulation where any nonzero element of $\nabla_{e}C$ becomes a source at its respective location on the Yee grid. Of course, since we use Tidy3D in the near-field regime, the terms corresponding to $\nabla_{e}C_{ff}$ must be first transformed from the far-field regime to the near-field regime (Figure 2d). The details of this transformation are explained in the Supporting Information. Once the corresponding near-field values of $\nabla_{e}C_{ff}$ are computed, they can be used as sources in the adjoint simulation that Tidy3D would solve (Figure 2e). To complete the setup for the backward simulation, the error source $\nabla_{e}C_{pf}$ also needs to be added at the original location of the quantum transition (Figure 2f). Once this setup is complete, the adjoining equation is solved for the metasurface modeled in the forward problem. Then, the necessary gradients are computed, and the tunable design parameters are updated. Repeating these steps in an iterative process enables optimization of an initial design for our desired behavior.

RESULTS

We use the presented optimization algorithm to design two metasurfaces both of the size $3\lambda \times 3\lambda \times 0.2\lambda$ (demonstrated in Figure 3a,d). While both aim to increase the Purcell factor of the embedded dipolar source by at least 1 order of magnitude at their design frequency $\lambda = 600$ nm, the first medium guides light along the axis perpendicular to it (the z-axis), and the second does so along a direction 40° off that axis.

For the light going out of the first medium, we expect to see a light cone similar to that in Figure 1d, and looking at the field intensities above the medium at different distances (Figure 3a), the formation of such a cone can clearly be seen. Furthermore, eq 1 described that the far-field pattern of the structure ($\tilde{y}_{(\theta,\phi)}$) was optimized by contrasting it with a ground truth pattern ($\tilde{y}_{t(\theta,\phi)}$). Figure 3b presents these parameters as 2D images that cover the upper hemisphere of the medium (θ and ϕ varying in the range $[0-\pi/2]$ and $[0-2\pi]$, respectively). Here, the ground truth is set to 1 for all values of ϕ, and θ values less than 10° and 0 elsewhere; and the far-field of the optimized medium is closely following this pattern. Figure 3c shows the radar pattern for the upper hemisphere at $\phi = 45°$, which is compatible with the expected objectives. Similarly, Figure 3d–f shows the same measures for the second structure. The medium is designed to direct light along a path with $\theta = 40°$ and $\phi = 140°$, with an approximately 10° cone angle. Figure 3e shows how well its performance compares to the ground truth, which is further upheld by the medium's radar pattern at $\phi = 140°$. Of course, it should be pointed out that although the depicted results only represent the performance in the upper hemisphere, the symmetry of the setup along the z axis means the lower hemisphere will mirror the same far-field behavior.

While the properties of the presented media are designed for the specific wavelength $\lambda = 600$ nm, the final designs presented those desired behaviors in a broader bandwidth. In Figure 4a,

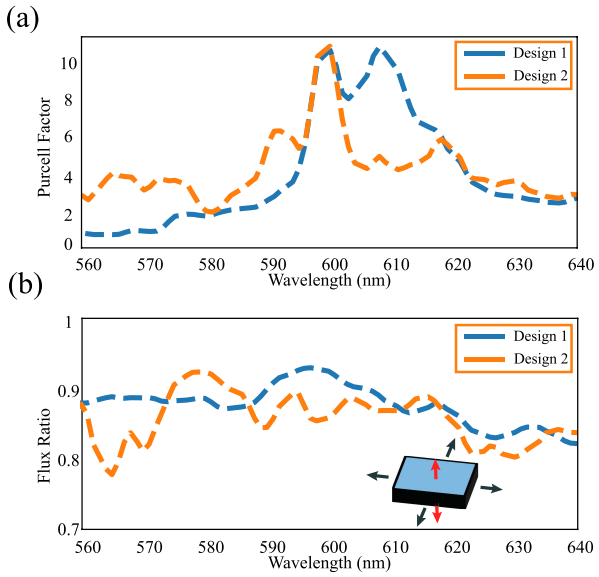

Figure 4. (a) Purcell factor as a function of the wavelength for the two designs (designs 1 and 2 guide the light at angles $\theta = 0°$ and $\theta = 40°$, respectively). (b) The ratio of the flux along the z axis on the large sides of the two media (red arrows) to the total outgoing flux from the medium (all arrows). The high ratio shows that the emitted photons have not been extracted to the guided mode, traveling along x/y axes.

we show the Purcell factors of the two structures. It is evident that, while better enhancement happens around 600 nm, at least a two-times improvement in the same measure holds for wavelengths 570–640 nm as well. This study shows that the designed media have indeed been successful in providing extra optical modes through which emitted photons can be extracted. However, for the purposes considered in this work, it is also paramount that the emitted light is not exclusively extracted into the bound modes of the pixelated *Si* slab and instead be predominantly guided out of the slab upward and downward. In order to evaluate these criteria, we then measured the ratio of the electromagnetic flux going along the z axis over the total flux escaping the metasurface. Of course, due to the large surface area of the up/down faces of the metasurface, we expect this ratio to be high; however, if the generated photons were unexpectedly being extracted into guided modes inside the metasurface, a significant portion of the outgoing flux would leak from the sides of the medium, and

https://doi.org/10.1021/acsomega.3c10362
ACS Omega 2024, 9, 24356−24361

this ratio would be very small. However, as Figure 4b demonstrates, this ratio is close to 1, showing that only a small portion of the extracted photons exits from the sides.

Finally, we delve deeper into the effect of the sizes of our structures on their light extraction and far-field performances. While previous works have demonstrated enhancement in light extraction with much smaller metasurface designs, the resulting devices were not as effective in guiding the extracted light in narrow directions. It can be intuitively construed that a larger design can provide the extra degrees of freedom required for focusing light on narrower beams. As a result, we expected that the light extraction enhancement would happen predominantly through the pixels closer to the source and that the pixels further away from it would have a more significant role in preserving the far-field behavior. However, trying to evaluate this hypothesis showed evidence to the contrary. For this evaluation, we started removing pixels further away from the source and modeling the behavior of the resulting device. Figure 5 shows the comparison between the far-field and its target performance (far-field ground truth), along with the PF enhancement at the central frequency for the reduced-size version of the first metasurface design. Panel (a) holds the full structure, while panels (b) and (c) keep a square area centered around the source, spanning $2.5\lambda \times 2.5\lambda$ and $1.8\lambda \times 1.8\lambda$, respectively. As expected, even removing a layer spanning two pixels from each side (Figure 5b) causes significant disruption in the far-field pattern. However, contrary to expectation, this also causes a noticeable drop in the Purcell factor, signifying the non-negligible role of the outer layers in enhancing the Purcell factor. Of course, the idea of an overall performance degradation as a result of removing elements of an optimized design is not unexpected either. We further examine the effect of changing metasurface sizes and the size of their building block pixels in the Supporting Information.

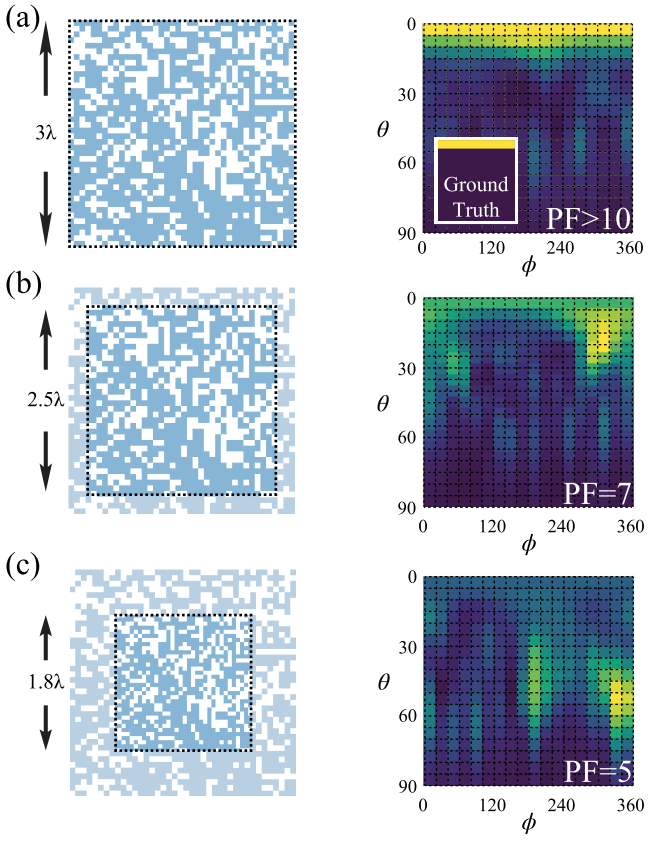

Figure 5. Effect of removing the outer-layer pixels of the optimized medium on photon emission directivity and Purcell factor. (a) Original design for photon emission normal to the metasurface with PF > 10, see Figure 3a–c for more details. (b) and (c) are the reduced-size versions of the original design in (a). The right column shows the corresponding comparison between the far-field and its target performance (ground truth), along with the PF enhancement at the central frequency.

CONCLUSIONS

This work discusses an approach for designing large-area all-dielectric metasurfaces for simultaneously enhancing light extraction and guiding light to specific directions in narrow angles. The multifaceted goal defined for this work necessitated the creation of a multiobjective design process capable of handling constraints in the far-field as well as the near-field region. As a result, we proposed an optimization process compatible with these requirements and employed it to design two different structures. These structures not only improve light extraction for a quantum transition placed inside them but also guide light into narrow cones along different directions. We then studied the spectral behavior of the designed media, which showed their relatively broadband capabilities. Finally, we examined the effect of the outer layers of the optimized design on its performance with regard to the two objectives defined for it. This showed the significant contribution the outer layers of the metasurface have on the enhancement of the Purcell factor as well as the formation of a narrow far-field beam.

ASSOCIATED CONTENT

Supporting Information

The Supporting Information is available free of charge at https://pubs.acs.org/doi/10.1021/acsomega.3c10362.

A detailed account of the equations describing the forward and backward passes of the inverse design process, along with a brief description of the materials available in the GitHub repository for this project (PDF)

AUTHOR INFORMATION

Corresponding Author

Erfan Khoram − *Department of Electrical and Computer Engineering, University of Wisconsin Madison, Madison, Wisconsin 53706, United States;* orcid.org/0000-0002-9921-5110; Email: ekhoram@wisc.edu

Authors

Zongfu Yu − *Department of Electrical and Computer Engineering, University of Wisconsin Madison, Madison, Wisconsin 53706, United States;* orcid.org/0000-0002-4536-1526

S. Ali Hassani Gangaraj − *Optical Physics Division, Corning Research and Development, Corning, New York 14831, United States;* orcid.org/0000-0003-1818-3215

Complete contact information is available at: https://pubs.acs.org/10.1021/acsomega.3c10362

Notes

The authors declare the following competing financial interest(s): Z.Y. is a co-founder of Flexcompute.

https://doi.org/10.1021/acsomega.3c10362
ACS Omega 2024, 9, 24356−24361

REFERENCES

(1) Gangaraj, S. A. H.; Ying, L.; Monticone, F.; Yu, Z. Enhancement of quantum excitation transport by photonic nonreciprocity. *Phys. Rev. A* **2022**, *106*, No. 033501.

(2) Ying, L.; Mattei, M. S.; Liu, B.; Zhu, S.-Y.; Goldsmith, R. H.; Yu, Z. Strong and long-range radiative interaction between resonant transitions. *Physical Review Research* **2022**, *4*, No. 013118.

(3) Pelton, M. Modified spontaneous emission in nanophotonic structures. *Nat. Photonics* **2015**, *9*, 427−435.

(4) Russell, K. J.; Liu, T.-L.; Cui, S.; Hu, E. L. Large spontaneous emission enhancement in plasmonic nanocavities. *Nat. Photonics* **2012**, *6*, 459−462.

(5) Noda, S.; Fujita, M.; Asano, T. Spontaneous-emission control by photonic crystals and nanocavities. *Nat. Photonics* **2007**, *1*, 449−458.

(6) Vučković, J.; Fattal, D.; Santori, C.; Solomon, G. S.; Yamamoto, Y. Enhanced single-photon emission from a quantum dot in a micropost microcavity. *Appl. Phys. Lett.* **2003**, *82*, 3596−3598.

(7) Choy, J. T.; Hausmann, B. J.; Babinec, T. M.; Bulu, I.; Khan, M.; Maletinsky, P.; Yacoby, A.; Lončar, M. Enhanced single-photon emission from a diamond−silver aperture. *Nat. Photonics* **2011**, *5*, 738−743.

(8) Trojak, O. J.; Park, S. I.; Song, J. D.; Sapienza, L. Metallic nanorings for broadband, enhanced extraction of light from solid-state emitters. *Appl. Phys. Lett.* **2017**, *111*, No. 021109.

(9) Jahani, S.; Jacob, Z. All-dielectric metamaterials. *Nature Nanotechnol.* **2016**, *11*, 23−36.

(10) Mohammadi Estakhri, N.; Edwards, B.; Engheta, N. Inverse-designed metastructures that solve equations. *Science* **2019**, *363*, 1333−1338.

(11) Qu, Y.; Zhou, M.; Khoram, E.; Yu, N.; Yu, Z. Resonance for analog recurrent neural network. *ACS Photonics* **2022**, *9*, 1647−1654.

(12) Yesilyurt, O.; Kudyshev, Z. A.; Boltasseva, A.; Shalaev, V. M.; Kildishev, A. V. Efficient topology-optimized couplers for on-chip single-photon sources. *ACS Photonics* **2021**, *8*, 3061−3068.

(13) Melo, E. G.; Eshbaugh, W.; Flagg, E. B.; Davanco, M. Multiobjective Inverse Design of Solid-State Quantum Emitter Single-Photon Sources. *ACS Photonics* **2023**, *10*, 959 DOI: 10.1021/acsphotonics.2c00929.

(14) Wambold, R. A.; Yu, Z.; Xiao, Y.; Bachman, B.; Jaffe, G.; Kolkowitz, S.; Choy, J. T.; Eriksson, M. A.; Hamers, R. J.; Kats, M. A. Adjoint-optimized nanoscale light extractor for nitrogen-vacancy centers in diamond. *Nanophotonics* **2020**, *10*, 393−401.

(15) Chung, H. Computational upper-limit of directional light emission in nano-LED via inverse design. *Opt. Express* **2022**, *30*, 9008−9020.

(16) Wiecha, P. R.; Arbouet, A.; Girard, C.; Lecestre, A.; Larrieu, G.; Paillard, V. Evolutionary multi-objective optimization of colour pixels based on dielectric nanoantennas. *Nature Nanotechnol.* **2017**, *12*, 163−169.

(17) Safdari, M. J.; Mirjalili, S. M.; Bianucci, P.; Zhang, X. Multi-objective optimization framework for designing photonic crystal sensors. *Appl. Opt.* **2018**, *57*, 1950−1957.

(18) Hammond, A. M.; Oskooi, A.; Chen, M.; Lin, Z.; Johnson, S. G.; Ralph, S. E. High-performance hybrid time/frequency-domain topology optimization for large-scale photonics inverse design. *Opt. Express* **2022**, *30*, 4467−4491.

(19) *Flex-Compute Tidy3D: FDTD for Electromagnetic Simulation*, https://flexcompute.com/tidy3d. (accessed Jan 2021).

(20) Novotny, L.; Hecht, B. *Principles of nano-optics*; Cambridge University Press, 2012.

(21) Barnes, W. Fluorescence near interfaces: the role of photonic mode density. *journal of modern optics* **1998**, *45*, 661−699.

(22) Newman, W. D.; Cortes, C. L.; Jacob, Z. Enhanced and directional single-photon emission in hyperbolic metamaterials. *JOSA B* **2013**, *30*, 766−775.

(23) Khoram, E.; Qian, X.; Yuan, M.; Yu, Z. Controlling the minimal feature sizes in adjoint optimization of nanophotonic devices using b-spline surfaces. *Opt. Express* **2020**, *28*, 7060−7069.

(24) Khoram, E.; Wu, Z.; Yu, Z. *Near-sensor and In-sensor Computing*; Springer, 2022; pp. 199−224.

(25) Khoram, E.; Chen, A.; Liu, D.; Ying, L.; Wang, Q.; Yu, Z.; et al. Nanophotonic Media for Artificial Neural Inference. *arXiv preprint arXiv:1810.07815* **2018**, DOI: 10.48550/arXiv.1810.07815.

(26) Taflove, A.; Hagness, S. C.; Piket-May, M. Computational electromagnetics: the finite-difference time-domain method. *Electrical Engineering Handbook* **2005**, *3*, 629−670.

https://doi.org/10.1021/acsomega.3c10362
ACS Omega 2024, 9, 24356−24361